Magnetic Resonance in Medicine 54:616–624 (2005)

Simulation of Anisotropic Growth of Low-Grade Gliomas Using Diffusion Tensor Imaging

Saâd Jbabdi,[1] Emmanuel Mandonnet,[2*] Hugues Duffau,[1,2] Laurent Capelle,[1,2] Kristin Rae Swanson,[3] Mélanie Pélégrini-Issac,[1] Rémy Guillevin,[4] and Habib Benali[1,5]

A recent computational model of brain tumor growth, developed to better describe how gliomas invade through the adjacent brain parenchyma, is based on two major elements: cell proliferation and isotropic cell diffusion. On the basis of this model, glioma growth has been simulated in a virtual brain, provided by a 3D segmented MRI atlas. However, it is commonly accepted that glial cells preferentially migrate along the direction of fiber tracts. Therefore, in this paper, the model has been improved by including anisotropic extension of gliomas. The method is based on a cell diffusion tensor derived from water diffusion tensor (as given by MRI diffusion tensor imaging). Results of simulations have been compared with two clinical examples demonstrating typical growth patterns of low-grade gliomas centered around the insula. The shape and the kinetic evolution are better simulated with anisotropic rather than isotropic diffusion. The best fit is obtained when the anisotropy of the cell diffusion tensor is increased to greater anisotropy than the observed water diffusion tensor. The shape of the tumor is also influenced by the initial location of the tumor. Anisotropic brain tumor growth simulations provide a means to determine the initial location of a low-grade glioma as well as its cell diffusion tensor, both of which might reflect the biological characteristics of invasion. Magn Reson Med 54: 616–624, 2005. © 2005 Wiley-Liss, Inc.

Key words: computational modeling; glioma; anisotropic growth; diffusion tensor; cell migration

Low-grade (WHO grade II) gliomas are initially slowly evolving tumors, but can become rapidly fatal after anaplastic transformation. Because of their infiltrative characteristics, surgery alone fails to cure these tumors, even in their premalignant stage. Indeed, these tumors may not form a solid mass but may invade diffusely throughout the brain parenchyma as "gliomatosis cerebri."

Recently, a biomathematical model (1) has been proposed to quantitatively describe the growth rates of gliomas visualized radiologically. This model takes into account the two major biological phenomena underlying the growth of gliomas at the cellular scale: proliferation and diffusion. The simplest choice for the proliferation term is a constant growth rate ρ, leading to an exponentially growing total number of glioma cells. For the invasive properties of gliomas, cell migration is assumed to be a random walk, corresponding to a passive (Fickian) diffusion characterized by a single coefficient D. Simulations of this proliferation–diffusion equation are performed on a 3D T_1 MR structural image of the brain, with segmentation of CSF (which corresponds to the boundaries of the parenchyma), white matter, and gray matter images.

In previous publications (2), the diffusion of cells in white matter is assumed to be 5 (to 100) times higher than in gray matter, consistent with observations that glioma cells migrate more quickly in white matter than in gray. Within white (or gray) matter, cell diffusion was considered an isotropic phenomenon. However, it is commonly accepted that glioma cells migrate preferentially along a direction favored by white matter fibers (3–7). The complex gross anatomical shape usually exhibited by low-grade gliomas is thought to be a direct consequence of this anisotropic cell diffusion.

In the past few years, diffusion tensor imaging (DTI) has emerged as a powerful tool to analyze the 3D geometry of white matter pathways. It allows the virtual in vivo dissection of white matter tracts (8–11) in healthy volunteers. Usefulness of DTI in the management of brain tumors is also under investigation (12). Determination of white matter tracts deformed by tumors appears to be a promising application for use in surgical planning (13).

In this paper, we propose to use DTI data for modeling anisotropic diffusion of cells and to show, by comparison between clinical data and results of simulation, how DTI data improves the diffusion–proliferation model of brain tumor growth.

The outline of this paper is as follows: first, we introduce the mathematical model that generalizes the diffusion–proliferation process of tumor growth and propose a numerical method to solve it. Simulations are then presented in the Results and compared to patient data. In the Discussion, the improvements brought by the model are highlighted and the limitations of the study are discussed, as well as the perspectives and the possible improvements that could be made in the future.

THEORY

Model

Different models of tumors growth in space and time have been proposed (14–17). In the case of infiltrative tumors such as low-grade gliomas, it is usual to model the evolution of cell concentration. Generally, tumor growth due to

[1]U678 INSERM/UPMC, Paris, France.
[2]CHU Pitié Salpêtrière-Service de Neurochirurgie, Paris, France.
[3]Pathology, University of Washington, Seattle, Washington, USA.
[4]CHU Pitié Salpêtrière-Service de Neuroradiologie, Paris, France.
[5]IFR49 Imagerie Neurofonctionnelle, Paris, France.

Grant sponsor: French ministry of Research; Grant number: ACI Neurosciences Computationelles et Intégratives 2002–2005 0220397; Grant sponsor: Faculté de Médecine Paris VI; Grant number: BQR 2004.

*Correspondence to: Emmanuel Mandonnet, CHU Pitié Salpêtrière, Service de Neurochirurgie, 47-83 Bd de l'Hôpital, 75634 Paris Cedex 13, France. E-mail: mandonnet@mac.com.

Received 19 August 2004; revised 8 April 2005; accepted 18 April 2005
DOI 10.1002/mrm.20625
Published online 8 August 2005 in Wiley InterScience (www.interscience.wiley.com).

net cell division can be represented by a differential equation in time,

$$\frac{\partial c}{\partial t} = f(c), \qquad [1]$$

where c is the glioma cell concentration and f is a function representing the temporal evolution pattern of the growth. For example, some functions f that have been used in other works are (14)

$$f(c) = \rho c \qquad \text{(exponential proliferation)} \qquad [2a]$$

$$f(c) = \rho c \frac{c - c_m}{c_m} \qquad \text{(Verhulst or logistic law)} \qquad [2b]$$

$$f(c) = \rho c \ln\left(\frac{c_m}{c}\right) \qquad \text{(Gompertz law),} \qquad [2c]$$

where ρ is an empirical modeling factor. For the exponential model, ρ is the relative increase of cell concentration per time unit. Spatial models, on the other hand, try to explain the spreading of tumor cells in space and the resulting shape of the glioma. The simplest way to represent cell migration is by assuming a Brownian-like random motion of cells, i.e., a diffusion process with some constant diffusion coefficient D.

Finally, the resulting partial differential equation (PDE) combines proliferation (time component) and infiltration (space component) of tumoral cells and states that the change in tumor concentration is the result of spatial spreading and cell division (15),

$$\frac{\partial c}{\partial t} = D\nabla^2 c + f(c), \qquad [3]$$

where ∇^2 is the Laplacian operator.

However, this model remains too simple because it does not take into account the heterogenous nature of the brain. Indeed, it has been observed that tumoral cells diffuse more rapidly in white matter than in gray matter (5). This tumor behavior has been previously addressed by adding a spatial dependence for the diffusion coefficient D, so that the rates of glioma cell migration depend on the location $\mathbf{x} = (x_i)_{i=1,3}$ in the brain (16),

$$\frac{\partial c}{\partial t} = \nabla.(D(\mathbf{x})\nabla c) + f(c), \qquad [4]$$

where $D(\mathbf{x}) = D_{\text{gray}}$ in gray matter and D_{white} in white matter and where ∇ is the gradient operator. We propose to further generalize this model to take into account not only the heterogeneity of the brain tissue but also its anisotropy, dealing with the fact that glioma cell migration is facilitated in the direction of white matter fibers. Equation [4] can be rewritten,

$$\frac{\partial c}{\partial t} = \nabla.(\mathbf{D}(\mathbf{x})\nabla c) + f(c), \qquad [5]$$

where $\mathbf{D}$ is the diffusion tensor that describes tumor cell diffusion, i.e., a 3-by-3 symmetric positive definite matrix that models the local anisotropy of the cell diffusion tensor. Thus, our model takes into account both location and direction within the structure of the brain tissue. The proliferation $f(c)$ is modeled in our simulations by a logistic law (Eq. [2b]) with $c_m = 10^5$ cells/mm^3.

To complete the model formulation, initial conditions are defined as $c(0, \mathbf{x}) = c_0(\mathbf{x})$ and, to inhibit migration of glioma cells outside of the brain tissue, $\mathbf{D}(\mathbf{x})\nabla c \cdot \mathbf{n} = 0$ for $\mathbf{x}$ on the sulcal and ventricular boundary of the brain, where $\mathbf{n}$ is the surface normal.

Implementation Issue

To solve Eq. [5], i.e., to estimate the cell density c, we propose using 3D finite differences (18), which consists of approximating temporal and spatial derivatives by their discrete expressions. First, considering the exponential model given in Eq. [2a] for the proliferation term in Eq. [5], we want to solve the following PDE,

$$\begin{cases} \dfrac{\partial c}{\partial t} = \nabla.(\mathbf{D}(\mathbf{x})\nabla c) + \rho c \\ c(0,\mathbf{x}) = c_0(\mathbf{x}) \end{cases}, \qquad [6]$$

where c_0 is the concentration of the tumoral cells at $t = 0$. Each part of this PDE is then discretized using ΔT as a time step and (ΔX, ΔY, ΔZ) as space steps. We obtain the following discrete equation,

$$\frac{C^{n+1} - C^n}{\Delta T} = \mathbf{A}C^n, \qquad [7]$$

where C^n is a vector representing cell density at the time $n\Delta T$ and $\mathbf{A}$ is a large sparse matrix representing discrete operators (the construction of this operator is developed in the Appendix). This is the forward Euler method. We use the θ-method instead of the forward Euler method in order to increase numerical stability. The θ-method consists of combining forward and backward numerical schemes (18), as follows:

$$\frac{C^{n+1} - C^n}{\Delta T} = (1 - \theta)\mathbf{A}C^n + \theta\mathbf{A}C^{n+1}, \qquad [8]$$

The choice of $\theta \in [0, 1]$ and ΔT is discussed in the Appendix.

Denoting $\delta^n = C^{n+1} - C^n$, we compute the cell concentration at time $(n + 1)\Delta T$ by first solving the equation

$$(\mathbf{I} - \theta\Delta T\mathbf{A})\delta^n = \Delta T\mathbf{A}C^n, \qquad [9]$$

where $\mathbf{I}$ is the identity matrix, which gives the value for δ^n. We use the preconstrained gradient method as implemented in Matlab® (The Mathworks) to solve this large sparse system and get the concentration C^{n+1} as

$$C^{n+1} = C^n + \delta^n \qquad [10]$$

Initial conditions are represented by a glial cell concentration C^0 in a voxel manually selected. A typical simulation

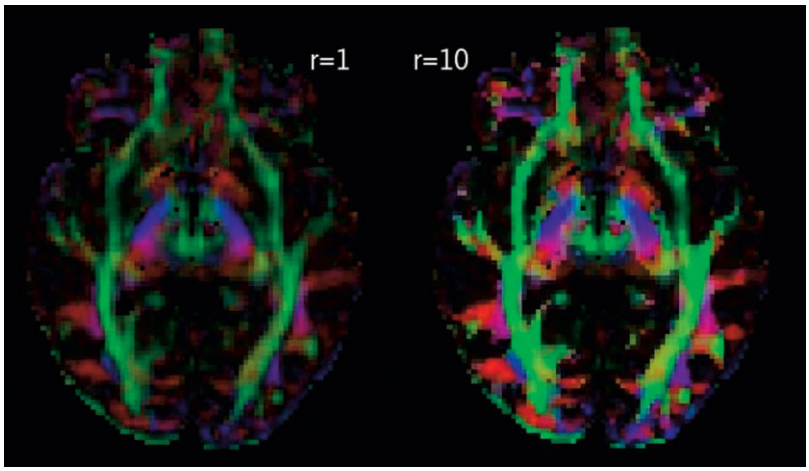

FIG. 1. RGB color maps of the tensor's principal diffusion directions. Left: tensor with no change in tumor cell diffusion anisotropy compared to water anisotropy ($r = 1$). Right: Tensor with change in tumor cell anisotropy ($r = 10$).

takes about 30 min on a 2.4-GHz processor with 2 GB of virtual memory.

MATERIALS AND METHODS

Patient Data

We selected MRIs of patients who had been followed for a WHO grade II glioma study at the Pitié Salpêtrière Hospital between 1994 and 2001. We focused on patients with tumors centered on the insula and extending into the temporal and/or frontal lobes because of the known anisotropy of the white matter in these regions. We followed the extension of the tumor on FLAIR (or T_2) sequences on serial images over months to years and before any specific treatment.

DTI Data Acquisition

Because there is no DTI atlas available, and no MRIs of the patients in a numerical format, the tumor growth simulations were done on a healthy subject data set (structural T_1 and DTI). Six gradient-weighted and one T_2-weighted image were acquired on a 1.5-T MR Scanner (GE Signa) using the following scan parameters: 128×128 image matrix, 2.03 mm in-plane pixel size; 3.5 mm slice thickness; $b = 1000$; (TR;TE) = (5000;91.8) ms; number of averages = 8. Thirty-six contiguous slices covering the whole brain were acquired. The total scanning time was approximately 14 min.

Tensor Preprocessing

Tensors were reconstructed as described in Ref. (19). For our simulations, we needed to artificially increase the anisotropy of white matter voxels. This modification is motivated by the fact that the interaction of tumoral cells with white matter fiber bundles is more complex than water diffusion. Indeed, glioma cells tend to attach and migrate along anatomical structures such as myelin (20), which could result in a higher anisotropy. Thus, we used DTI data to provide tensor directionality, but we modified the water diffusion values.

Let $(\lambda_i, e_i)_{i=1,2,3}$ denote the eigenvalues and eigenvectors of the water diffusion tensor **D.** We used the following transformed tensor **D** to represent the diffusion tensor of tumor cells:

$$\bar{\mathbf{D}} = \bar{\lambda}_1(r)e_1e_1^T + \bar{\lambda}_2(r)e_2e_2^T + \bar{\lambda}_3(r)e_3e_3^T. \quad [11]$$

This operation modifies the eigenvalues of the tensor, but not the eigenvectors, which implies that the tensor orientation is preserved while the diffusion values along the principal axes and the anisotropy are changed. The transformation is controlled by a parameter r. When r equals 1, the tensor is not changed. $r < 1$ corresponds to a decrease in anisotropy and $r > 1$ to an increase in anisotropy. We detail in the Appendix how we chose the functions $\bar{\lambda}_i(r)$, taking the shape of the tensor and the fiber crossing issue into account. The effect of the in-

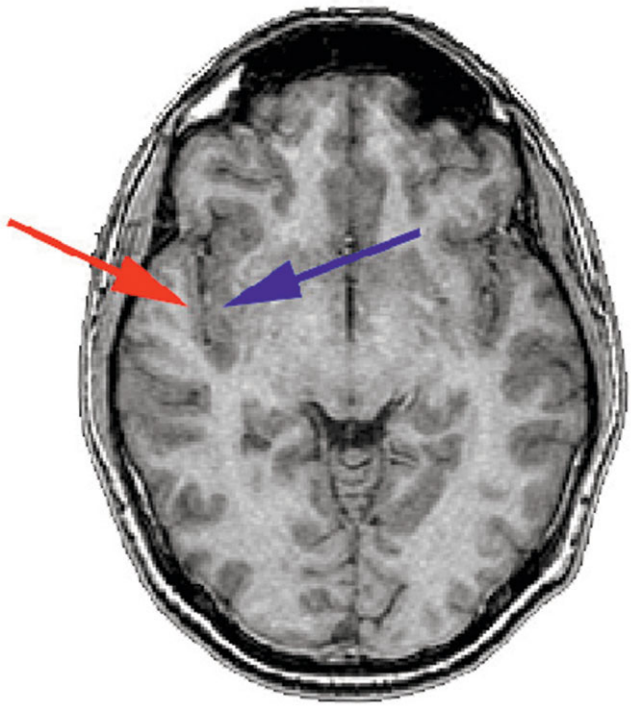

FIG. 2. Starting location of the simulations. The blue (resp., red) arrow indicates a starting point located in the insular (resp., temporal) part of the uncinate fasciculus.

crease in anisotropy can be seen on the RGB image in Fig. 1 representing the principal diffusion directions (21).

Choice of Parameters

The proliferation parameter ρ was set to the constant value of $\rho = 0.0012\ \text{day}^{-1}$, corresponding to the observed growth rate of high-grade gliomas divided by 10, to approximate the growth rate of low-grade gliomas (16, 17, 22).

For the cell diffusion tensor **D,** we keep a fivefold difference between the mean diffusion in gray and white matter: $D_{\text{white}} = 5D_{\text{gray}}$ as previously reported (16). D_{white} and D_{gray} are not known exactly because many tumors involve both gray and white matter. Therefore, we estimated D_{white} and D_{gray} using the total mean diffusion empirically observed for typical tumors that contain both gray and white matter. The total mean diffusion was estimated based on two facts. First, Mandonnet et al. (23), in a study of patients suffering from low-grade gliomas, reported that the diameter of the detectable part of the tumor expands about 4 mm per year. Second, one can show that the detectable diameter d obeys the asymptotic law (15)

$$d(t) \sim 4\sqrt{D\rho}\ t, \qquad [12]$$

for large time t, where D is the mean cell diffusion and ρ the net proliferation constant for an exponential proliferation law. Thus, we take $D = 7.5 \times 10^{-3}\ \text{mm}^2\ \text{day}^{-1}$, which is the value corresponding to a detectable diameter growing of 4 mm per year and a proliferation rate of $\rho = 0.0012\ \text{day}^{-1}$. This value corresponds to the mean of gray matter and white matter diffusion under the assumption that the tumor contains equal amounts of white and gray matter, so by simple algebra, and assuming $D_{\text{white}} = 5D_{\text{gray}}$, we have $D_{\text{white}} = 10^{-2}\ \text{mm}^2\ \text{day}^{-1}$ and $D_{\text{gray}} = 2.10^{-3}\ \text{mm}^2\ \text{day}^{-1}$.

RESULTS

The aim of this study is to simulate tumor growth in a normal brain to best fit patient data, given the preprocessed DTI data obtained from a normal subject. The results were visually compared to patient MRIs. For all the simulations, the initial concentration c_0 was set to 200 cells/mm^3 in one voxel. The cell density threshold of detection was set to 500 cells/mm^3. Actually, the value of this threshold influences the duration before the tumor is apparent on simulated MRI images, but neither the kinetics of the extension of the tumor front nor the shape of the tumor is affected.

We first performed growth simulations to analyze the shape on MRI of the gliomas. Figure 3 shows the comparison between a clinical MRI at diagnosis and the results of both isotropic and anisotropic simulations. We assumed that the tumor started to grow in the inferior part of the insula (see initial voxel indicated by a blue arrow in Fig. 2). The shape of the tumor on the patient's MRI (Fig. 3a) is better fitted by the anisotropic simulation (Fig. 3b) rather than the isotropic one (Fig. 3c). This is especially true for the posterior extension in the temporal lobe, corresponding to the invasion of the inferior fronto-occipital fasciculus and the optic radiations. We have increased the diffusion tensor anisotropy by varying the parameter r (r = 5, 10, 20, 100). The best "de visu" fit was obtained for a value of $r = 10$.

We have also launched the simulation from a voxel situated in the temporal part of the uncinate fasciculus (Fig. 2). The resulting tumor shape more poorly reproduced the real scan (Fig. 4a), proving the sensitivity of the shape to initial voxel selection. On the contrary, isotropic simulation was not dramatically changed by this second initial voxel (Fig. 4b).

We also tested the model to describe the kinetics of tumor growth. We selected a patient with a tumor spreading along the arcuate fasciculus (Figs. 5 and 6), with two MRI scans at an interval of 7 years (and without any specific treatment during this period). The results show that ρ and **D** model the tumor growth well, but does not show a clear advantage of using the anisotropic model.

Finally, considering a constant product $D_{\bullet\rho}$, we have tuned the ratio D_{white}/ρ, between 5 and 35 mm^2. As already mentioned in Ref. (24), this ratio is related to the width of the cell density profile. Indeed, for small values of this ratio, the cell density profile is sharp, with a rapid decrease of cell density beyond the detection threshold. For high values, this profile is very broad, leading to an aspect of gliomatosis on MRI (when the density exceeds the threshold value). Interestingly, the ratio has only minor influence on the shape of the tumors.

DISCUSSION

Summary of Previous Work

Computational modeling of glioma growth by a proliferation–diffusion equation was initiated 10 years ago. It has been used to quantify the effect of chemotherapy on an anaplastic astrocytoma (15), to analyze the effect of extent of surgical resection on survival curves (17), and to suggest a classification based on differential individual values of D and ρ (22). A refinement of the model was proposed by Swanson et al (2, 25). for high-grade gliomas. They used a segmented MRI atlas of the brain as a virtual medium for simulations, allowing differential motility in gray and white matter. This model gives a good understanding of the radiological evolution of high-grade gliomas. To date, this model has not been used to simulate low-grade glioma growth. The development of this new version, including anisotropic diffusion along white matter tracts as given by DTI, was motivated by the fact that MRI patterns of low-grade gliomas exhibited complex shapes that were not predicted by an isotropic model.

Anisotropic Diffusion

In this work, DTI information was used in a 3D MRI atlas to include anisotropic diffusion in a proliferation–diffusion model of brain tumor growth. This anisotropic diffusion is mandatory to fit correctly the shape of the lesion seen on MRI. Indeed, even with a differential motility between white and gray matter, it is not possible isotropically to obtain a tumor shape as in Fig. 3, at least not with a single voxel as the initial state. In this case of the anisotropic proliferation diffusion model, the tumor shape reflects the invaded fasciculi: the uncinate, the inferior fron-

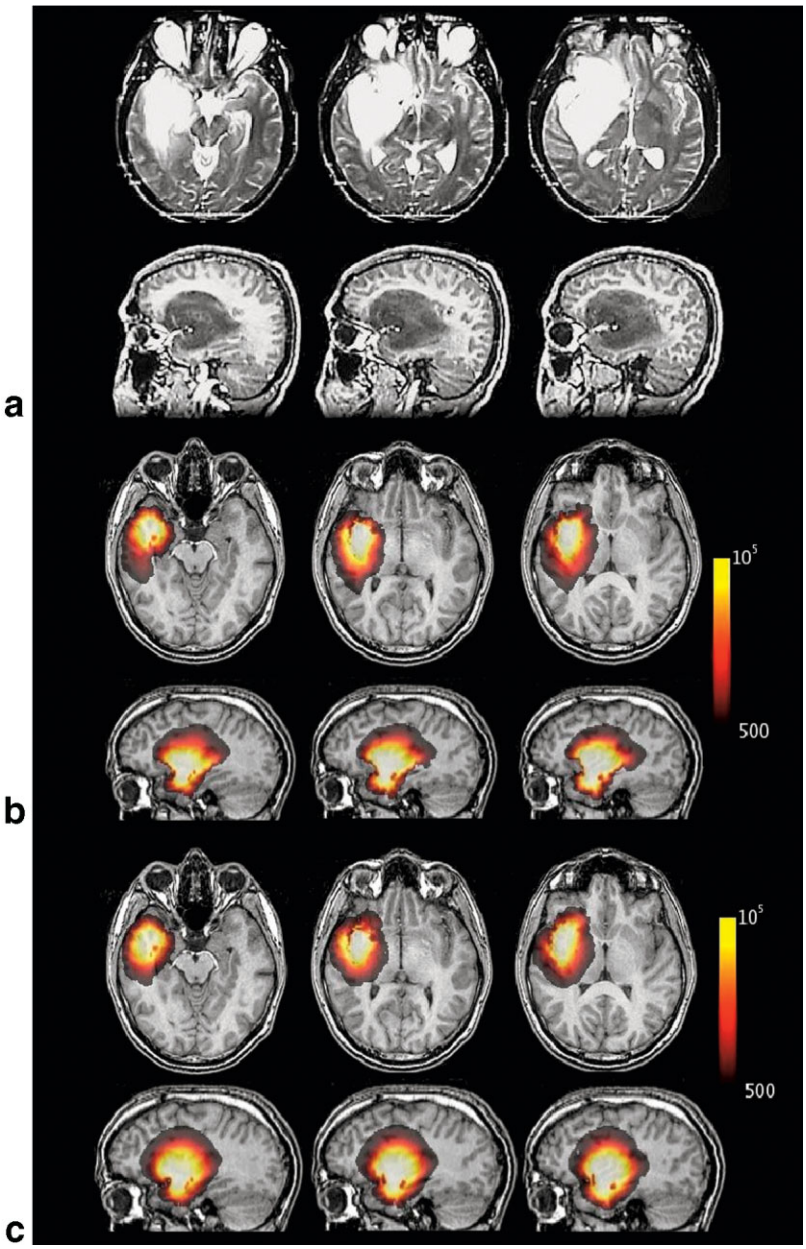

FIG. 3. Simulations with a starting point located in the insular part of the uncinate fasciculus. (**a**) Patient data. (**b**) Anisotropic simulations ($r = 10$). (**c**) Isotropic simulations. Visualization threshold : 500 cells per mm^3.

to-occipital, and the optic radiations. Moreover, the anisotropy of cell diffusion tensor must be increased to fit correctly the clinically observed shape of the tumors. From a microscopic point of view, this result is not so surprising, because we do not expect such different objects as a water molecule (estimated by DTI) and a glial cell to have the same diffusive behavior. Indeed, cell migration along fiber tracts is the result of complex interactions, including facilitated or active diffusion, which we model by simply increasing the tensor anisotropy by a factor *r*. To our knowledge, this is the first report of an experimentally defined value for the anisotropic glioma cell invasion along the directions described by diffusion tensor imaging.

Influence of the Initial Location of the Tumor

In this study, we restricted our simulations to a single initial voxel. This hypothesis seems reasonable because real low-grade gliomas rarely exhibit multifocal tumors. However, when successive MRIs are available, one could define the initial state by considering the first scan (26). In this case, the problem of multiple initial voxels is no longer relevant.

We have also shown that different locations of the initial voxel lead to different shapes and different evolutions of the tumor. Thus, it should be possible to use this model to determine the starting location of the tumor. This is important because it is believed that tumor location correlates with other characteristics, such as the genetic molecular profile (27, 28).

Limitations and Questions Raised by the Present Model

We have observed that many fasciculi were invaded in the simulations, whereas real tumors spread only over one or two fasciculi. For example, the simulated tumor starting in

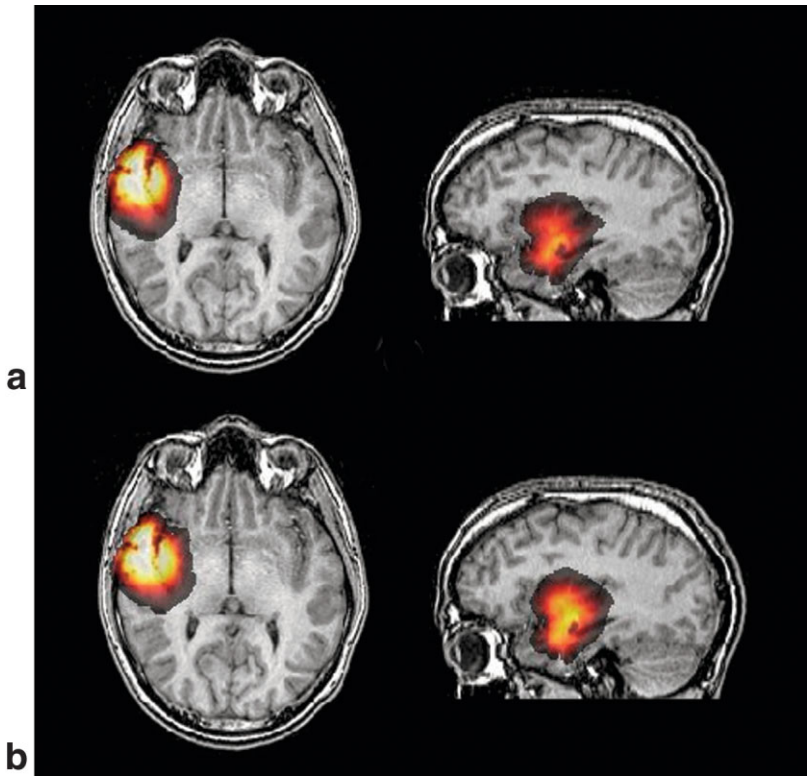

FIG. 4. Anisotropic (**a**) and isotropic (**b**) simulations with a starting point located in the temporal part of the uncinate fasciculus (red arrow in Fig.2).

the arcuate fasciculus invaded all the fasciculi of this region: arcuate, of course, but also inferior longitudinal fasciculus, whereas real tumors spread only along the arcuate fasciculus. This discrepancy between simulations and clinical data suggests that there may exist some underlying biological interaction between tumoral cells and a specific fasciculus that are not taken into account by this model.

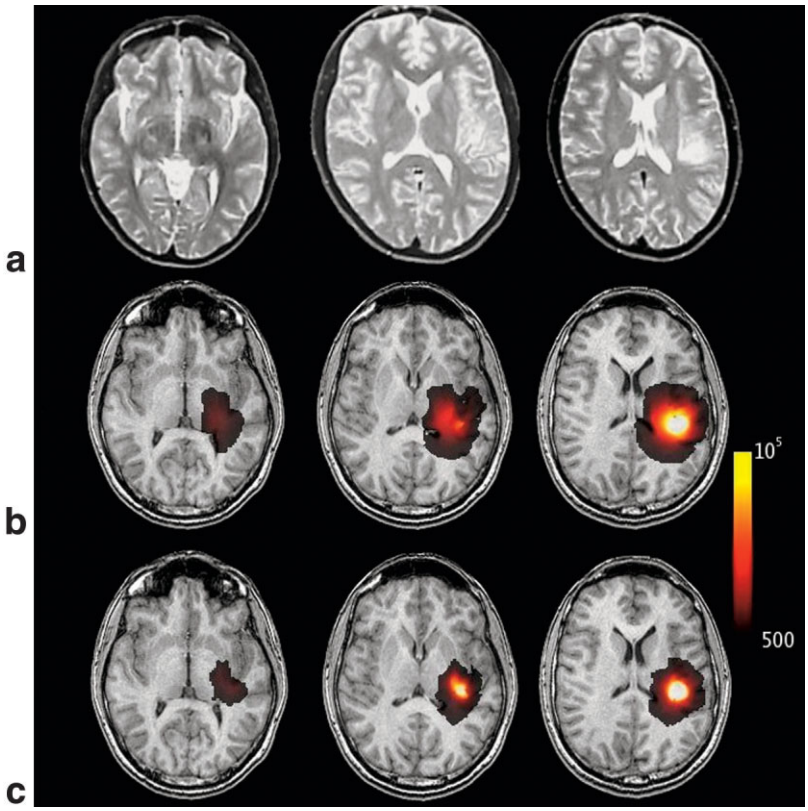

FIG. 5. (**a**) First MRI for patient data with tumor within the arcuate fasciculus. (**b**) Corresponding image for the isotropic simulation. (**c**) Corresponding image for the anisotropic simulation. Visualization threshold : 500 cells per mm^3.

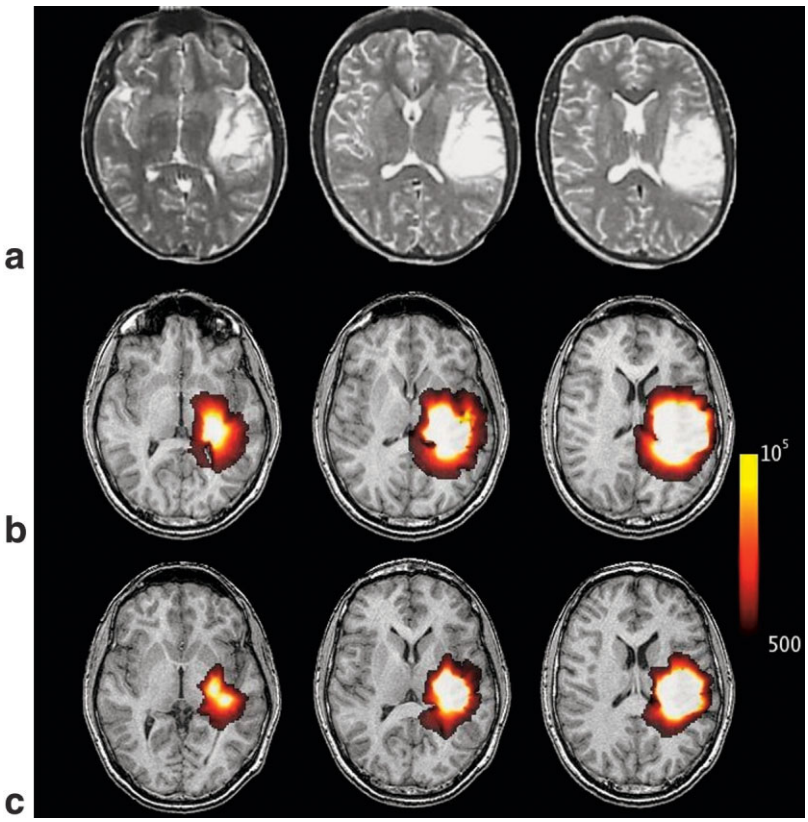

FIG. 6. (**a**) MRI of the same patient, after 7 years of evolution. (**b**) Isotropic simulation after 7 years of propagation. (**c**) Anisotropic simulation ($r = 10$). Visualization threshold : 500 cells per mm^3.

In the present model, mass effect is not taken into account. Consequently, we use DTI data from a given normal data set. This approach makes sense because many low-grade gliomas usually do not show any significant mass effect on MRI. Actually, during the final process of this work, we discovered that other authors were independently performing a similar work on high-grade gliomas (29). These authors also added a mechanical model for the bulk part of glioblastoma, inducing mass effect and deformation of parenchyma. For low-grade gliomas with mass effect, deformation of surrounding parenchyma should be included in the model. A more complex work would also calculate the changes in DTI data due to brain deformation.

Because no standard DTI atlas is available, we have used the data coming from a healthy subject. For the brain segmentation, we used an automated method (implemented in SPM2[6]) based on gray levels. This method does not allow a perfect delineation of the subarachnoidal spaces. For example, in the case of the tumor spreading along the arcuate fasciculus, there were small bridges of gray matter in our mask (unlike in the real brain) that spanned the two edges of the sylvian valley, allowing the diffusion from one cortex to the other. In real tumors, the arachnoid, which constitutes an anatomical barrier, stops this mechanism of extension. Thus, it is of great importance to segment carefully the brain mask, separating its different structures and barriers, which requires a good spatial resolution for the DTI acquisition.

[6]http://www.fil.ion.ucl.ac.uk/spm/spm2.html.

The values of some parameters are only approximations, because there is a lack of clinical data. As already discussed, the cell density threshold of detection on MRI has been set to 500 cells/mm^3. This value has been estimated on comparison of histology and CT. There is no study aiming to measure this threshold for the different MRI signals. The ratio D/ρ is also poorly known. To go a step further, it would be necessary to analyze tumor cell density on serial stereotactic biopsies, even in an invisible, but probably invaded, area on MRI. This is very difficult for many reasons. First, it is questionable, for ethical reasons, to do a biopsy of a radiologically normal tissue. Second, even if such biopsies were available, anatomopathological methods are still unable to reliably count isolated tumor cells. Note that different MRI signals revealing different measures of tumor extent would constitute an interesting alternative to solve this problem.

CONCLUSION

Using the proliferation–diffusion model, we have shown in this paper that anisotropic diffusion based on DTI data enhances the accuracy of simulation of the growth of low-grade glioma. Several improvements of the present model will be implemented in the near future. First, an algorithm is required for automated (or semi-automated) determination of the starting location of the tumor. Likewise, a systematic way should be developed to determine the diffusion, proliferation, and anisotropy parameters, allowing the best fit with a radiological evolution of at least three successive images. These improvements are required to envisage a longitudinal

clinical study testing the practical usefulness of this sophisticated tool. The goal of the study would be to estimate the prognostic values of the different parameters, which could also be helpful to optimize therapeutic strategies. Finally, if the predictive value of the simulations (at least during the premalignant phase) is proven, this model would provide a new way to quantify treatment effects of low-grade tumors, whose long survival times render randomized clinical trials very difficult to organize.

ACKNOWLEDGMENTS

We thank the two anonymous reviewers whose comments helped to improve the paper. The Authors thank Dr. Thien Huong N'Guyen for kindly providing us with the diffusion data and Robert Costalat and Olivier Pantz for helpful discussions.

APPENDIX

Finite Differences

Let $c(t,\mathbf{x})$ denote the cell concentration at time t and location $\mathbf{x}$ of the space. Developing Eq. [5] leads to the equation

$$\frac{\partial c}{\partial t} = \sum_{i,j=1}^{3} D_{ij} \frac{\partial^2 c}{\partial x_i \partial x_j} + \sum_{i=1}^{3} \tilde{D}_i \frac{\partial c}{\partial x_i} + \rho c, \qquad [A1]$$

where

$$\tilde{D}_i = (\mathbf{D}\nabla)_i = \sum_{j=1}^{3} \frac{\partial \mathbf{D}_{ij}}{\partial x_j}. \qquad [A2]$$

$\tilde{D}$ is derived from the tensor $\mathbf{D}$ by computing its element-by-element gradient. Let $c(n\Delta T,i\Delta X,j\Delta Y,k\Delta Z) \equiv C^n_{i,j,k}$ and let C^n denote the vectorized version of $C^n_{i,j,k}$, we use the following discrete schemes for computing the derivatives:

$$\frac{\partial c}{\partial t} \rightarrow \frac{C^{n+1}_{i,j,k} - C^n_{i,j,k}}{\Delta T}$$

$$\frac{\partial c}{\partial x} \rightarrow \frac{C^n_{i+1,j,k} - C^n_{i-1,j,k}}{2\Delta X}$$

$$\frac{\partial^2 c}{\partial x^2} \rightarrow \frac{C^n_{i+1,j,k} - 2C^n_{i,j,k} + C^n_{i-1,i,j,k}}{\Delta X^2}$$

$$\frac{\partial^2 c}{\partial x \partial y} \rightarrow \frac{C^n_{i+1,j+1,k} + C^n_{i-1,j-1,k} - C^n_{i+1,j-1,k} - C^n_{i-1,j+1,k}}{4\Delta X \Delta Y} \qquad [A3]$$

and similarly for $\frac{\partial c}{\partial y}, \frac{\partial c}{\partial z}, \frac{\partial^2 c}{\partial y^2}, \frac{\partial^2 c}{\partial z^2}, \frac{\partial^2 c}{\partial x \partial z},$ and $\frac{\partial^2 c}{\partial y \partial z}$.

We obtain the following discrete expression for Eq. [5]:

$$\frac{C^{n+1}_{i,j,k} - C^n_{i,j,k}}{\Delta T} = \mathrm{D}_{11} \frac{C^n_{i+1,j,k} - 2C^n_{i,j,k} + C^n_{i-1,j,k}}{\Delta X^2}$$

$$+ \mathrm{D}_{22} \frac{C^n_{i,j+1,k} - 2C^n_{i,j,k} + C^n_{i,j-1,k}}{\Delta Y^2} + \mathrm{D}_{33} \frac{C^n_{i,j,k+1} - 2C^n_{i,j,k} + C^n_{i,j,k-1}}{\Delta Z^2}$$

$$+ 2\mathrm{D}_{12} \frac{C^n_{i+1,j+1,k} + C^n_{i-1,j-1,k} - (C^n_{i+1,j-1,k} + C^n_{i-1,j+1,k})}{4\Delta X \Delta Y}$$

$$+ 2\mathrm{D}_{13} \frac{C^n_{i+1,j,k+1} + C^n_{i-1,j,k-1} - (C^n_{i+1,j,k-1} + C^n_{i-1,j,k+1})}{4\Delta X \Delta Y}$$

$$+ 2\mathrm{D}_{23} \frac{C^n_{i,j+1,k+1} + C^n_{i,j-1,k-1} - (C^n_{i,j+1,k-1} + C^n_{i,j-1,k+1})}{4\Delta X \Delta Y}$$

$$+ \tilde{\mathrm{D}}_1 \frac{C^n_{i+1,j,k} - C^n_{i-1,j,k}}{2\Delta X} + \tilde{\mathrm{D}}_2 \frac{C^n_{i,j+1,,k} - C^n_{i,j-1,k}}{2\Delta Z}$$

$$+ \tilde{\mathrm{D}}_3 \frac{C^n_{i,j,k+1} - C^n_{i,j,k-1}}{2\Delta Z} + \rho C^n_{i,j,k} \qquad [A4]$$

which can be rewritten as

$$\frac{C^{n+1} - C^n}{\Delta T} = AC^n, \qquad [A5]$$

where $\mathbf{A}$ is a big sparse matrix with 19 diagnonal element and where elements of $\mathbf{A}$ depend on $\mathbf{D}$, $\tilde{D}$, ρ, and on the space/time discretization stepsizes (ΔT, ΔX, ΔY, ΔZ).

To fit the best solution, we must choose the algorithm parameters ΔT and θ with care. If we neglect the diffusion term in Eq. [8], we obtain the scheme

$$\frac{C^{n+1} - C^n}{\Delta T} = (1-\theta)\rho C^n + \theta\rho C^{n+1}$$

$$C^{n+1} = \frac{1 - \rho\Delta T\theta + \rho\Delta T}{1 - \rho\Delta T\theta} C^n \qquad [A6]$$

Denoting $u = \rho\Delta T$, we obtain the following solution for an initial condition C^0:

$$C^n = \left(\frac{1 - \theta u + u}{1 - \theta u}\right)^n C^0. \qquad [A7]$$

The analytical solution for this exponential proliferation law is $C^n = C^0\, e^{n\rho\Delta T}$, leading to the relation

$$\left(\frac{1 - \theta u + u}{1 - \theta u}\right)^n = e^{nu}, \qquad [A8]$$

which gives a relationship between the parameters

$$\theta = \frac{1}{u} - \frac{1}{e^u - 1} = \frac{1}{\rho\Delta T} - \frac{1}{e^{\rho\Delta T} - 1}. \qquad [A9]$$

In this case, the diffusion D is zero.

Tensor Transform

In order to achieve the tensor transformation, we need to define three indices that give information about the shape of the tensor. Let c_l, c_p, and c_s be, respectively, the linear, planar and spherical indices for the tensor, defined by (30)

$$c_l = \frac{\lambda_1 - \lambda_2}{\lambda_1 + \lambda_2 + \lambda_3},\ c_p = \frac{2(\lambda_2 - \lambda_3)}{\lambda_1 + \lambda_2 + \lambda_3},\ c_s = \frac{3\lambda_3}{\lambda_1 + \lambda_2 + \lambda_3}, \quad [A10]$$

where the eigenvalues are sorted in decreasing order ($\lambda_1 \geq \lambda_2 \geq \lambda_3$). These indices have a simple interpretation: $c_l \sim 1$ means that the tensor is linear, i.e., there is a single dominating diffusion direction. A planar tensor $c_p \sim 1$ occurs when there is a mixture of two equivalent diffusion directions. $c_s \sim 1$ is the isotropic tensor case.

To increase the tensor anisotropy without changing its orientation, one can simply multiply the largest eigenvalue by a factor r and reconstruct the tensor as

$$\bar{\mathbf{D}} = r\lambda_1 e_1 e_1^T + \lambda_2 e_2 e_2^T + \lambda_3 e_3 e_3^T. \quad [A11]$$

However, when fiber crossing occurs in a voxel, more than one diffusion direction is to be favored. In the planar case ($c_p = 1$), we wish to prevent from diffusing in the direction normal to the plane defined by (e_1, e_2). In the spherical case ($c_s = 1$), no direction is preferred; the tensor should not be changed. These different cases may be summarized by the following tensor change,

$$\bar{\mathbf{D}} = a_1(r)\lambda_1 e_1 e_1^T + a_2(r)\lambda_2 e_2 e_2^T + a_3(r)\lambda_3 e_3 e_3^T, \quad [A12]$$

where the vector $(a_i)_i$ is defined by

$$\begin{pmatrix} a_1 \\ a_2 \\ a_3 \end{pmatrix} = \begin{pmatrix} r & r & 1 \\ 1 & r & 1 \\ 1 & 1 & 1 \end{pmatrix} \begin{pmatrix} c_l \\ c_p \\ c_s \end{pmatrix}. \quad [A13]$$

The anisotropy change is controlled by the factor r. Note that for $r = 1$, the tensor is not changed. This is because the shape indices sum up to 1: $c_l + c_p + c_s = 1$. When $c_l = 1$, only the eigenvalue along the main diffusion direction is changed (multiplied by r), while the two largest eigenvalues are modified when $c_p = 1$. The tensor is not changed when $c_s = 1$. The eigenvalues of the transformed tensor are defined by $\bar{\lambda}_i(r) = a_i(r)\lambda_i$. In order to insure that the mean diffusion is not affected by this increase of anisotropy, the transformed tensor is multiplied by a scalar value,

$$\bar{\mathbf{D}} \rightarrow \frac{\text{trace}(\mathbf{D})}{\Sigma_k \bar{\lambda}_k} \bar{\mathbf{D}}. \quad [A14]$$

REFERENCES

1. Swanson KR, Bridge C, Murray JD, Alvord EC Jr. Virtual and real brain tumors: using mathematical modeling to quantify glioma growth and invasion. J Neurol Sci 2003;216:1–10.
2. Swanson KR, Alvord EC Jr, Murray JD. A quantitative model for differential motility of gliomas in grey and white matter. Cell Prolif 2000;33:317–329.
3. Belien AT, Paganetti PA, Schwab ME. Membrane-type 1 matrix metalloprotease (mt1-mmp) enables invasive migration of glioma cells in central nervous system white matter. J Cell Biol 1999;144:373–384.
4. Giese A, Westphal M. Glioma invasion in the central nervous system. Neurosurgery, 1996;39:235–250.
5. Giese A, Bjerkvig R, Berens ME, Westphal M. Cost of migration: invasion of malignant gliomas and implications for treatment. J Clin Oncol 2003;21:1624–1636.
6. Pedersen PH, Edvardsen K, Garcia-Cabrera I, Mahesparan R, Thorsen J, Mathisen B, Rosenblum ML, Bjerkvig R. Migratory patterns of lac-z transfected human glioma cells in the rat brain. Int J Cancer 1995. 62:767–771.
7. Yoshida D, Watanabe K, Noha M, Takahashi H, Teramoto A, Sugisaki Y. Tracking cell invasion of human glioma cells and suppression by anti-matrix metalloproteinase agent in rodent brain-slice model. Brain Tumor Pathol 2002;19:69–76.
8. Conturo T, Lori N, Cull T, Akbudak E, Snyder A, Shimony J, McKinstry R, Burton H, Raichle M. Tracking neuronal fiber pathways in the living human brain. Proc Natl Acad Sci USA 1999;96:10422–10427.
9. Basser P, Pajevic S, Pierpaoli C, Duda J, Aldroubi A. In vivo fiber tractography using DT-MRI data. Magn Reson Med 2000;44:625–632.
10. Poupon C, Clark CA, Frouin V, Regis J, Block I, Le Bihan D, Mangin JF. Regularization of diffusion-based direction maps for the tracking of brain white matter fascicles. NeuroImage 2000;12:184–195.
11. Catani M, Howard RJ, Pajevic S, Jones DK. Virtual in vivo interactive dissection of white matter fasciculi in the human brain. Neuroimage 2002;17:77–94.
12. Sundgren PC, Dong Q, Gomez-Hassan D, Mukherji SK, Maly P, Welsh R. Diffusion tensor imaging of the brain: review of clinical applications. Neuroradiology 2004;46:339–350.
13. Mori S, Frederiksen K, van Zijl P, Stieltjes B, Kraut M, Solaiyappan M, Pomper M. Brain white matter anatomy of tumor patients evaluated with diffusion tensor imaging. Ann Neurol 2002;51:377–380.
14. Marusic M, Bajzer Z, Freyer JP, Vuk-Palovic S. Analysis of growth of multicellular tumour spheroids by mathematical models. Cell Prolif 1994;27:73–94.
15. Tracqui P, Cruywagen GC, Woodward DE, Bartoo GT, Murray JD, Alvord EC Jr. A mathematical model of glioma growth: the effect of chemotherapy on spatio-temporal growth. Cell Prolif 1995;28:17–31.
16. Swanson KR. Mathematical modeling of the growth and control of tumors. Ph.D. thesis, University of Washington, 1999.
17. Woodward DE, Cook J, Tracqui P, Cruywagen GC, Murray JD, Alvord EC Jr. A mathematical model of glioma growth: the effect of extent of surgical resection. Cell Prolif 1996;29:269–288.
18. Raviart PA, Thomas JM. Introduction à l'analyse des équations aux dérivées partielles. Masson, Paris, 1983.
19. Bammer R, Burak A, Moseley ME. In vivo MR tractography using diffusion imaging. Eur J Radiol 2002;45:223–234.
20. Giese A, Kluwe L, Laube B, Meissner H, Berens ME, Westphal M. Migration of human glioma. Neurosurgery 1996;38:755–764.
21. Douek P, Turner R, Pekar J, Patronas N, Le Bihan D. MR color mapping of myelin fiber orientation. J Comp Assist Tomogr 1991;15:923–929.
22. Burgess PK, Kulesa PM, Murray JD, Alvord EC Jr. The interaction of growth rates and diffusion coefficients in a three-dimensional mathematical model of gliomas. J Neuropathol Exp Neurol 1997;56:704–713.
23. Mandonnet E, Delattre JY, Tanguy ML, Swanson KR, Carpentier AF, Duffau H, Cornu P, Van Effenterre R, Alvord EC Jr, Capelle L. Continuous growth of mean tumor diameter in a subset of grade II gliomas. Ann Neurol 2003;53:524–528.
24. Swanson KR, Alvord EC Jr, Murray JD. Virtual resection of gliomas: effects of location and extent of resection on recurrence. Math Comput Model 2003;37:1177–1190.
25. Swanson KR, Alvord EC Jr, Murray JD. Virtual brain tumours (gliomas) enhance the reality of medical imaging and highlight inadequacies of current therapy. Br J Cancer 2002;86:14–18.
26. Tracqui P, Mendjeli M. Modelling 3-dimensional growth of brain tumours from time series of scans. Math Models Methods Appl Sci 1999;9:581–598.
27. Zlatescu MC, Tehrani Yazdi A, Sasaki H, Megyesi JF, Betensky RA, Louis DN, Cairncross JG. Tumor location and growth pattern cor- relate with genetic signature in oligodendroglial neoplasms. Cancer Res 2001;61:6713–6715.
28. Mueller W, Hartmann C, Hoffmann A, Lanksch W, Kiwit J, Tonn J, Veelken J, Schramm J, Weller M, Wiestler OD, Louis DN, Von Deimling A. Genetic signature of oligoastrocytomas correlates with tumor location and denotes distinct molecular subsets. Am J Pathol 2002;161:313–319.
29. Clatz O, Bondiau PY, Delinguette H, Sermesant M, Warfield SK, Malandain G, Ayache N. Brain tumor growth simulation. Tech Rep 5187, Inria, April 2004.
30. Westin CF, Maier SE, Mamata H, Nabavi A, Kikinis JR. Processing and visualization for diffusion tensor MRI. Med Image Anal 2002;6:93–108.